THE JOURNAL OF PHYSICAL CHEMISTRY LETTERS
A JOURNAL OF THE AMERICAN CHEMICAL SOCIETY

pubs.acs.org/JPCL

Letter

The Evolution from Superatom- to Plasmon-Mediated Magnetic Circular Dichroism in Colloidal Metal Nanoparticles Spanning the Nonmetallic to Metallic Limits

Juniper Foxley, Thomas D. Green, Marcus A. Tofanelli, Christopher J. Ackerson, and Kenneth L. Knappenberger, Jr.*

Cite This: *J. Phys. Chem. Lett.* 2023, 14, 5210−5215

Read Online

ACCESS | Metrics & More | Article Recommendations | Supporting Information

ABSTRACT: The magneto-optical absorption properties of colloidal metal nanoclusters spanning nonmetallic to metallic regimes were examined using variable-temperature variable-field magnetic circular dichroism (VTVH-MCD) spectroscopy. Charge neutral $Au_{25}(SC_8H_9)_{18}$ exhibited MCD spectra dominated by Faraday C-terms, consistent with expectations for a nonmetallic paramagnetic nanocluster. This response is reconciled by the open-shell superatom configuration of $Au_{25}(SC_8H_9)_{18}$. Metallic and plasmon-supporting $Au_{459}(pMBA)_{170}$ exhibited temperature-independent VTVH-MCD spectra dominated by Faraday A-terms. $Au_{144}(SC_8H_9)_{60}$, which is intermediate to the metallic and nonmetallic limits, showed the most complex VTVH-MCD response of the three nanoclusters, consisting of 19 distinguishable peaks spanning the visible and near-infrared (3.0−1.4 eV). Variable-temperature analysis suggested that none of these transitions originated from plasmon excitation. However, evidence for both paramagnetic and mixed (i.e., nondiscrete) transitions of $Au_{144}(SC_8H_9)_{60}$ was observed. These results highlight the complexity of gold nanocluster electronic transitions that emerge as sizes approach metallic length scales. Nanoclusters in this regime may provide opportunities for tailoring the magneto-optical properties of colloidal nanostructures.

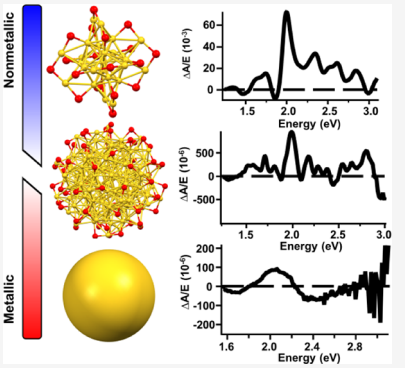

Gold nanostructures are subject to a great deal of study due to their potential applications as photonic, therapeutic, or catalytic material.[1−6] The optical and electronic properties of these structures are influenced by their size, composition, and morphology, allowing for several potential degrees of freedom by which these systems can be tailored to meet specific applications.[7,8] One area of particular interest involves understanding the magneto-optical responses of gold nanostructures, which provide opportunities for polarization-selective applications, such as chiral catalysis, spin dynamics, and chiroptical spectroscopy.[9] An effective method for studying magneto-optical extinction properties is magnetic circular dichroism (MCD), which describes changes to the dichroic response of a material upon application of a magnetic field. Here, we report on the MCD responses of a series of colloidal gold nanostructures that span the nonmetallic and metallic limits. Our distinction between these two categories is the difference between so-called discrete (nonmetallic) and collective (metallic) electronic excitation.

The dominant optical feature of metallic gold nanoparticles is the localized surface plasmon resonance (LSPR). In general, metallic colloidal nanoparticles show distinct MCD responses that depend on the order of the photoexcited LSPR mode. For example, a single asymmetric derivative response is observed in isotropic gold nanospheres, which support a dipolar plasmon mode.[10] This observation contrasts with nanostructures that support higher order plasmons, such as the quadrupolar modes of colloidal nanoprisms and nanodecahedra. In these cases, the quadrupolar excitation has a clearly distinct Gaussian MCD response.[11] Similarly, gold nanorods show mode-specific MCD responses. The nanorod transverse LSPR shows a derivative line shape, similar to that observed for nanospheres, whereas the longitudinal LSPR shows a Gaussian MCD response.[12] However, this Gaussian response arises as a consequence of the low rotational symmetry about the transverse axis of the nanorod, unlike the order-dependent response observed in nanoprisms or nanodecahedra.[12] Taken together, these examples show the potential for using nanoparticle structure to controllably modulate the amplitude and polarization of light transmission.

Contrasting with the collective plasmon excitations that are hallmarks of metallic nanostructures, nonmetallic nanocluster MCD spectra exhibit many peaks that are affected by factors such as spin−orbit coupling, zero-field splitting of electronic

Received: April 29, 2023
Accepted: May 25, 2023
Published: May 31, 2023

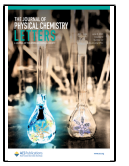

https://doi.org/10.1021/acs.jpclett.3c01170
J. Phys. Chem. Lett. 2023, 14, 5210−5215

fine structure states, valence electronic configurations, and ligand-field symmetry considerations.[9,12−18] For example, the $Au_9(PPh_3)_8^{3+}$ and $Au_{25}(SC_8H_9)^-$ nanocluster ions display several distinct MCD absorption features.[13−15] Further work has used magnetic circular photoluminescence (MCPL), the emission analogue of MCD, to obtain a more complete description of the magneto-optical responses of specific clusters. One such investigation focused on the emissive states of $Au_{25}(SC_8H_9)_{18}$, which allowed photoluminescence originating from metal−metal and metal-to-ligand transitions to be distinguished.[17,18] Work on systems of intermediate size suggests a complicated change in magneto-optical properties as plasmon-supporting domains are approached. For example, in the $Au_{102}(pMBA)_{44}$ nanocluster, a temperature-dependent variance in the Landé g factor has been investigated, showing a distinct change from diamagnetic to paramagnetic character with increasing temperature. This effect has been primarily attributed to a rehybridization of the d and sp bands due to lattice-based expansion and contraction, which causes changes in the electron vacancies at higher temperatures.[16] Although larger than the 9- and 25-metal-atom nanoclusters, the $Au_{102}(pMBA)_{44}$ species is still a nonmetallic system. As such, there exists a knowledge gap regarding the evolution of magneto-optical properties in the size range intermediate to the nonmetallic and metallic limits.

In order to help fill this gap, we have measured and compared the variable-temperature variable-field magnetic circular dichroism (VTVH-MCD) spectra for $Au_{25}(SC_8H_9)_{18}$, $Au_{144}(SC_8H_9)_{60}$, and $Au_{459}(pMBA)_{170}$ monolayer-protected nanoclusters (MPCs). MPCs are a class of structurally well-defined colloidal metal nanoparticles, and as such, provide an ideal platform for examining the size dependence of nanoscale gold magneto-optical signals. The MPCs studied here span a size range from 0.9 nm ($Au_{25}(SC_8H_9)_{18}$) to 2.4 nm ($Au_{459}(pMBA)_{170}$).[19] $Au_{25}(SC_8H_9)_{18}$ was chosen because it is nonmetallic, and its electronic configuration is accurately described using superatomic models.[20] Furthermore, $Au_{25}(SC_8H_9)_{18}$ can be converted between diamagnetic and paramagnetic behavior by oxidation, similar to other molecular metal−ligand complexes.[21,22] Hence, molecular-like MCD responses can be expected for $Au_{25}(SC_8H_9)_{18}$. In contrast, $Au_{459}(pMBA)_{170}$ is plasmonic and clearly in the metallic regime.[19] $Au_{144}(SC_8H_9)_{60}$ is an MPC that shows both metallic and nonmetallic behavior. For example, $Au_{144}(SC_8H_9)_{60}$ shows electrochemical charging trends consistent with metallic nanoparticles.[23] Electron−phonon scattering rates of $Au_{144}(SC_8H_9)_{60}$ likewise follow two-temperature model predictions for a metallic Fermi gas.[24] Pair distribution function analysis of powder X-ray diffraction of $Au_{144}(SC_8H_9)$, however, suggests that the cluster is polymorphic, where one polymorph contains Au atoms arranged in an icosahedral (nonmetallic) arrangement and a second form contains multiply twinned fcc crystallites (metallic).[25] Temperature-dependent absorption and single-crystal X-ray diffraction results show nonmetallic character in $Au_{144}(SC_8H_9)_{60}$.[26,27] Additional studies have observed that the transient dynamics of $Au_{144}(SC_8H_9)_{60}$ display power independence and are interpreted to indicate that the cluster is nonmetallic.[28,29] A definitive transition to metallic properties appears to occur somewhere between 144 and 187 gold atoms.[30] Taken together, these results indicate $Au_{144}(SC_8H_9)_{60}$ is an excellent candidate for studying magneto-optical properties for domains on the verge of metallicity. Our results reveal complex low-temperature MCD spectra for $Au_{144}(SC_8H_9)_{60}$ most consistent with nonmetallic character.

Spectrally resolved MCD signal, $\Delta A/E$, can be understood in terms of Faraday A-, B-, and C-terms, which describe the effect of the applied magnetic field on excited states (A-term), ground states (C-term), and mixing between states (B-term). The MCD response is given as

$$\frac{\Delta A}{E} = \gamma \mu_B \vec{H}\left[A\left(-\frac{\partial f(E)}{\partial E}\right) + \left(B + \frac{C}{k_B T}\right) f(E)\right] \quad (1)$$

Where γ is the gyromagnetic ratio, μ_B is the Bohr magneton, k_B is the Boltzmann constant, T is the sample temperature in Kelvin, $\vec{H}$ is the applied magnetic field strength, $f(E)$ is a function describing the line shape, and A, B, and C refer to the respective Faraday terms.[31] The A-term reflects Zeeman splitting in the excited state, which leads to a derivative-shaped peak in the MCD spectrum. The B-term results from field-induced mixing of states and is generally observed as a Gaussian peak shape. The magnitude of this effect is inversely proportional to the energy separation of the states involved. Since the energy separation of electronic states tends to decrease as energy increases, the B-term typically (but not exclusively) reflects mixing of excited states. Both the A- and B-terms are temperature-independent under most circumstances. The C-term reflects Zeeman splitting of the ground state and is only observed for systems with an unpaired spin (i.e., $S \neq 0$).[32] This term is temperature-dependent, since the relative population of the Zeeman-split fine structure states of the ground state depends on thermal energy. At low temperatures and/or high applied field strengths such that $\mu_B \vec{H} \gg k_B T$, C-terms dominate the MCD spectrum of paramagnetic systems.

The absorbance and MCD spectra of $Au_{459}(pMBA)_{170}$ are shown in Figure 1a,b. The 1.6-K absorption spectrum is plotted versus excitation energy from 1.6−3.0 eV (Figure 1a), and the MCD spectra obtained at 10-T applied field strength and several sample temperatures are overlaid (Figure 1b). The $Au_{459}(pMBA)_{170}$ absorption spectrum contained a single Gaussian peak with an approximate mean excitation energy

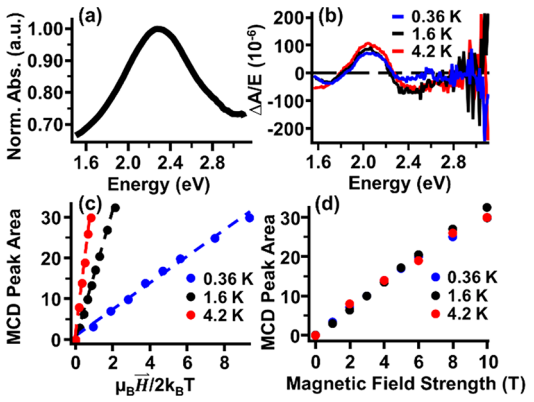

Figure 1. Absorption spectrum measured at 1.6 K (a) and subtracted MCD spectra displaying the bisignate response at 10 T (b) of $Au_{459}(pMBA)_{170}$ are shown. MCD spectra exhibit a bisignate response at all temperatures (0.36, 1.6, and 4.2 K) similar to the observed response of an LSPR in larger nanospheres. VTV $\vec{H}$-MCD studies at 0.36, 1.6, and 4.2 K reveal linear (c) and temperature-independent (d) magnetization responses, supporting assignment to a plasmon excitation.

https://doi.org/10.1021/acs.jpclett.3c01170
J. Phys. Chem. Lett. 2023, 14, 5210−5215

of 2.3 eV, which was attributed to a localized surface plasmon resonance. At all sample temperatures, $Au_{459}(pMBA)_{170}$ MCD spectra contained a single peak superimposed on a linearly increasing background signal (Figure S1). Previous reports on the MCD from plasmonic nanospheres have shown that the spectrum in this energy range contains a single asymmetric A-term. Subtraction of the background signal from the $Au_{459}(pMBA)_{170}$ MCD measurements yielded a bisignate spectral response that resembled an A-term (Figure 1b). The zero crossing of the $Au_{459}(pMBA)_{170}$ bisignate MCD response agreed well with the energy of the LSPR absorption peak (Figure 1a). Next, to compare the MCD response of $Au_{459}(pMBA)_{170}$ to plasmonic nanoparticles, the temperature-dependent MCD response was analyzed. The VTVH-MCD response is shown, plotted as the MCD intensity vs $\mu_B\vec{H}/2k_BT$ in Figure 1c. As expected for a nonparamagnetic system, the VTVH response is linear at 0.36, 1.6, and 4.2 K. The temperature independence of the $Au_{459}(pMBA)_{170}$ response is further verified by overlaying the MCD intensity vs applied field strength for all three temperatures in the Figure 1d. The three linear data sets overlay, confirming the MCD temperature independence of the $Au_{459}(pMBA)_{170}$ plasmon excitation. The MCD signal of the metallic $Au_{459}(pMBA)_{170}$ provides a reference to which the $Au_{25}(SC_8H_9)_{18}$ and $Au_{144}(SC_8H_9)_{60}$ responses can be compared.

The $Au_{25}(SC_8H_9)_{18}$ and $Au_{144}(SC_8H_9)_{60}$ 10-T MCD absorption spectra are plotted for several sample temperatures along with the 1.6-K linear absorption spectrum for each cluster in Figures 2, S2, and S3. In contrast to the

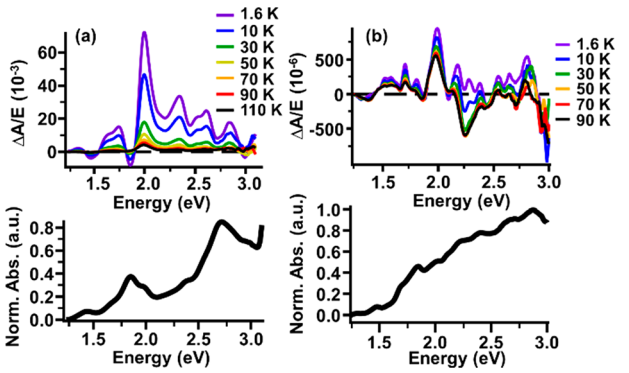

Figure 2. MCD (top) and absorption spectra (bottom) measured at 10 T and several sample temperatures for $Au_{25}(SC_8H_9)_{18}$ (a) and $Au_{144}(SC_8H_9)_{60}$ (b). Multiple distinct peaks arising in the MCD of $Au_{144}(SC_8H_9)_{60}$ were qualitatively more similar to the magneto-optical response of $Au_{25}(SC_8H_9)_{18}$ than the plasmon-dominant response of $Au_{459}(pMBA)_{170}$.

$Au_{459}(pMBA)_{170}$ response, VTVH-MCD results for both $Au_{25}(SC_8H_9)_{18}$ and $Au_{144}(SC_8H_9)_{60}$ nanoclusters show strong sensitivity to sample temperature. The prominence of the temperature dependence reflects the contribution of Faraday C-terms to the VTVH-MCD signal, which is not observed in the magneto-optical spectra for plasmonic excitation (Figure 1). Another clear distinction between the low-temperature MCD response of $Au_{25}(SC_8H_9)_{18}$ and $Au_{144}(SC_8H_9)_{60}$ when compared to $Au_{459}(pMBA)_{170}$ is the large number of distinct peaks spanning 1.4−3.0 eV for the smaller nanoclusters. In the case of $Au_{25}(SC_8H_9)_{18}$ (Figure 2a), 12 different peaks are resolved in this energy range. The large difference between $Au_{25}(SC_8H_9)_{18}$ and $Au_{459}(pMBA)_{170}$ is expected, as $Au_{25}(SC_8H_9)_{18}$ is typically considered to be a more "molecular-like" nanocluster with an inorganic diameter of approximately 9 Å.[33] Moreover, charge neutral $Au_{25}(SC_8H_9)_{18}$ is known to be paramagnetic, which would predict a temperature-dependent MCD response dominated by Faraday C-term contributions.[21] However, the striking contrast between $Au_{144}(SC_8H_9)_{60}$ and $Au_{459}(pMBA)_{170}$ is unexpected. $Au_{144}(SC_8H_9)_{60}$ has a complex geometric structure that includes a 114-gold-atom "grand core", which is the internal kernel of the nanocluster, and an additional 30 gold atoms located in a metal-chalcogenide "shell" that combine to form a 1.8 nm inorganic diameter.[26,34] Therefore, a high density of electronic states is expected for $Au_{144}(SC_8H_9)_{60}$. Furthermore, $Au_{144}(SC_8H_9)_{60}$ exhibits electron dynamics and electrochemical charging behaviors consistent with metallic nanoparticles.[23,24,35] The fact that $Au_{144}(SC_8H_9)_{60}$ exhibited 19 distinct MCD peaks spanning 1.4−3.0 eV was consistent with the previously observed emergence of distinct peaks in the absorption spectrum at low temperatures.[27] $Au_{144}(SC_8H_9)_{60}$ also displayed temperature-dependent magneto-optical responses qualitatively more similar to $Au_{25}(SC_8H_9)_{18}$ than $Au_{459}(pMBA)_{170}$, providing support for the dominance of single-electron excitations (Figure 2b).

While previously published low-temperature absorption spectra suggest a large number of individual excitation features, analysis of the VTVH-MCD signal allows for a more complete understanding of the spectra. For example, VTVH-MCD can be used to identify paramagnetic centers and mixing between states that contribute to electronic excitations. In order to quantitatively characterize the $Au_{25}(SC_8H_9)_{18}$ and $Au_{144}(SC_8H_9)_{60}$ magneto-optical signals, the VTVH-MCD signal intensities obtained throughout the visible for both $Au_{25}(SC_8H_9)_{18}$ (Figure 3a) and $Au_{144}(SC_8H_9)_{60}$ (Figure 3b)

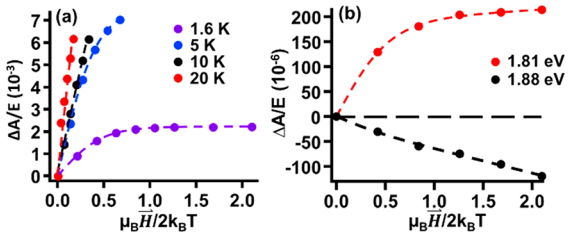

Figure 3. VTV $\vec{H}$-MCD of $Au_{25}(SC_8H_9)_{18}$ (a) and $Au_{144}(SC_8H_9)_{60}$ (b). $Au_{25}(SC_8H_9)_{18}$ magnetization curves are taken at 1.75 eV, corresponding to the LUMO ← HOMO − 1 excitation region. A saturating response gives way to a linear response at around 10 K, supporting assignment to an open-shell (seven-electron) superatom P state. $Au_{144}(SC_8H_9)_{60}$ displays similar saturation behavior at 1.81 eV, suggesting a paramagnetic initial state. However, excitation at 1.88 eV displays a higher contribution of the Faraday B-term, displaying a notable change in magneto-optical response for transitions separated by less than 100 meV in excitation energy.

were analyzed at several sample temperatures. The relationship between the measured MCD intensity and temperature can be understood from the following expression:

$$I_{VTVH} = I\left(\frac{\mu_B\vec{H}}{2k_BT}\right) = C_0\tanh\left(\frac{g\mu_B\vec{H}}{2k_BT}\right) + B_0\vec{H} \quad (2)$$

where g is the Landé g factor, μ_B is the Bohr magneton, k_B is the Boltzmann constant, T is the sample temperature in Kelvin,

https://doi.org/10.1021/acs.jpclett.3c01170
J. Phys. Chem. Lett. 2023, 14, 5210−5215

$\vec{H}$ is the applied magnetic field strength, and C_0 and B_0 refer to the Faraday C- and B-terms, respectively.[32] Of these, the Landé g factor describes the spin, orbital, and total angular momentum resulting from spin−orbit coupling of a given state. In instances where $g\mu_B\vec{H} < 2k_BT$ and $B_0 \approx 0$, the MCD intensity will increase linearly as $\vec{H}$ increases, with g serving as a constant of proportionality between the applied field and the observed signal magnitude. However, when $g\mu_B\vec{H} > 2k_BT$ and $B_0 \approx 0$, the MCD intensity will saturate at a magnitude determined by the Landé g-factor, exhibiting no additional increases with $\vec{H}$. This low-temperature MCD saturation is a hallmark of a paramagnetic transition. When $B_0 \neq 0$, the Faraday B-term will contribute a linear-field-dependent increase to MCD signal strength with no dependence on sample temperature. The B_0 and C_0 terms describe the relative contributions of linear and saturation-based magnetization behavior, respectively, which can allow for the determination of the magnetic character and degree of field-induced mixing of a feature.[36,37] At sample temperature of 1.6 K, both $Au_{25}(SC_8H_9)_{18}$ and $Au_{144}(SC_8H_9)_{60}$ exhibited the saturation behavior predicted from eq 2, indicating paramagnetic responses for both nanoclusters (Figure 3). Hence, the current VTVH-MCD data (Figure 3b) provide the first experimental evidence for a paramagnetic response from $Au_{144}(SC_8H_9)_{60}$. This assignment would not be possible from the low-temperature absorption spectra shown in Figure 3b or reported in reference 27.

The saturation behavior observed for the 1.6-K MCD field dependence of $Au_{25}(SC_8H_9)_{18}$ can be understood from superatom models. According to superatom theory, stable nanoclusters occur for "magic" stoichiometries that achieve closed electronic valence shells. For electrons in an isotropic potential, the energy levels of the system ascend as $1S^2$, $1P^6$, $1D^{10}$, and so on, corresponding to shell closings for 2, 8, and 18 net valence electrons, respectively.[38,39] For thiolated nanoclusters of general formula $Au_N(SR)_M^z$, where z is the formal charge, the number of valence electrons, n, is determined as $n = N - M - z$.[40] Since each Au atom contributes one 6s valence electron and each thiol ligand localizes a valence electron in a bond, the anionic $Au_{25}(SC_8H_9)_{18}^-$ species is especially stable, corresponding to a superatom P ground state ($n = 25 - 18 + 1 = 8$). Indeed, theoretical calculations support this interpretation of $Au_{25}(SC_8H_9)_{18}^-$ stability. Oxidation of $Au_{25}(SC_8H_9)_{18}^-$ to a neutral charge state generates an open-shell, seven-electron superatom that can correspond to either $S = 1/2$ or $S = 3/2$.[21] Density functional calculations predict strong spin−orbit coupling for the superatom P ground state, predicting a ^2P term.[41] Electron paramagnetic resonance and magnetic circular photoluminescence measurements confirm the paramagnetic behavior of the $Au_{25}(SC_8H_9)_{18}$ ground state.[18,21] Fitting the $Au_{25}(SC_8H_9)_{18}$ 1.6-K MCD isotherm (Figure 3a) intensity field dependence using eq 2 is consistent with excitation from a paramagnetic superatom P term. Using eq 2, Landé g-factors spanning values of 1.4 ± 0.1 to 2.0 ± 0.2 (Table S1) were obtained for the VTVH-MCD peaks in the region of the $Au_{25}(SC_8H_9)_{18}$ HOMO−LUMO energy gap (1.4−1.9 eV). The values obtained from experimental data agree well with expectations for a superatom $^2P_{3/2}$ ($g = 1.33$) or $^4P_{5/2}$ ($g = 1.6$) ground state. Raising the $Au_{25}(SC_8H_9)_{18}$ sample temperature from 1.6 to 10 and 20 K yields linear VTVH-MCD isotherms (Figure 3a); the 5-K isotherm showed signs of saturation at the largest field strengths. This phenomenon, by which VTVH-MCD isotherms convert from a saturating to nonsaturating profile with increasing sample temperature, is referred to as nesting.[32] The observed nesting for $Au_{25}(SC_8H_9)_{18}$ is likely the result of a thermally assisted population of the HOMO fine structure states at higher temperatures (5−20 K). The slope of the for $Au_{25}(SC_8H_9)_{18}$ 1.6-K VTVH-MCD isotherm is zero for $\frac{\mu_B\vec{H}}{k_BT} > 1$. This observation is expected for an MCD response dominated by Faraday C-terms and suggested magnetic-field-induced mixing was minimal for this transition. Based on the onset of saturation observed for large applied fields at 5 K, it is suggested that the lower bound for the Landé g-factor of the 1.75 eV transition was 1.5. Hence, the VTVH-MCD isotherms for $Au_{25}(SC_8H_9)_{18}$ validate assignment of the magneto-optical response as originating from transitions from an open-shell (seven-electron) superatom P ground state.

The $Au_{144}(SC_8H_9)_{60}$ MCD temperature dependence is more complicated than that observed for $Au_{25}(SC_8H_9)_{18}$. For example, the spectral profile for excitation energies greater than 2.2 eV changed dramatically as the sample temperature was raised above 10 K. This change in the measured spectrum may have resulted from expansion or structural rearrangement of the nanocluster.[34,42] As a result of this dramatic change in spectra, we have restricted the VTVH-MCD analysis to 1.6-K isotherms for transitions at energies less than 2.0 eV. In particular, we focus on a pair of peaks that span the 1.75−1.90 eV excitation range. Of the pair, the lowest energy peak (1.81 eV mean energy) shows a clear saturating behavior, indicative of a paramagnetic initial state (Figure 3b). The Landé g-factor for this transition is 1.6 ± 0.3. Based on available theory, the 1.81 eV excitation should include transitions from sulfur atom orbitals as well as contributions from the superatom D orbital.[43] Due to a linear field dependence clearly evident at large field strengths, the best fit to the 1.88 eV 1.6-K isotherm required both Faraday B- and C-terms to obtain an appropriate fit. Both the 1.81 and 1.88 eV VTVH-MCD isotherms had nonzero slopes for $\frac{\mu_B\vec{H}}{k_BT} > 1$, suggesting magnetic-field-induced mixing contributed to these transitions. Strong field-induced mixing contributions are evidence of the influence of multiple states contributing to the feature. Due to this, while the presence of a temperature-dependent MCD response and a paramagnetic center suggests a single-electron excitation, the influence of a manifold of states implies that the feature is not discrete. The complexity of the $Au_{144}(SC_8H_9)_{60}$ optical response therefore arises not only from the number of individual peaks but also the manifold of states from which each originate, which cannot be extracted from the low-temperature absorption spectra. The Landé g-factor determined for the 1.88 eV C-term contribution was 2.0 ± 0.8. The large contribution from the B-term along with spectral overlap of neighboring peaks results in large error bars for this assignment. It is expected that both superatom D states and transitions based in the metal kernel contribute to this transition.[43] The striking difference in the VTVH-MCD isotherms for two peaks colocated within 100 meV is noteworthy, given the proximity of $Au_{144}(SC_8H_9)_{60}$ with respect to the onset of both structural and geometric metallicity.

https://doi.org/10.1021/acs.jpclett.3c01170
J. Phys. Chem. Lett. 2023, 14, 5210−5215

In summary, the low-temperature magnetic circular dichroism absorption of three colloidal gold monolayer-protected nanoclusters—$Au_{25}(SC_8H_9)_{18}$, $Au_{144}(SC_8H_9)_{60}$, and $Au_{459}(pMBA)_{170}$—was described. These three systems were chosen for study because they span the molecular ($Au_{25}(SC_8H_9)_{18}$) to metallic ($Au_{459}(pMBA)_{170}$) domains, including a nanocluster considered intermediate to these limits ($Au_{144}(SC_8H_9)_{60}$). The $Au_{459}(pMBA)_{170}$ nanocluster exhibited bisignate MCD spectra, consistent with a dipolar localized surface plasmon excitation. The paramagnetic charge neutral $Au_{25}(SC_8H_9)_{18}$ showed saturating variable-field MCD isotherms for 1.6-K sample temperatures. The saturating behavior is reconciled by the open-shell, seven-valence-electron configuration of the superatom P ground state of this nanocluster. $Au_{144}(SC_8H_9)_{60}$ showed the most striking MCD spectrum of the three nanoclusters, consisting of 19 distinct magnetically responsive peaks. The $Au_{144}(SC_8H_9)_{60}$ MCD spectrum consisted of a diversity of field responses, including signatures of both paramagnetism and field-induced mixing. The VTVH-MCD results for $Au_{144}(SC_8H_9)_{60}$ showed that many of the observed peaks did not result from discrete transitions but instead were heavily influenced by mixing between states. The identification of paramagnetic and mixed transitions was uniquely resolved by VTVH-MCD and could not be inferred from low-temperature absorption measurements. The results indicate that $Au_{144}(SC_8H_9)_{60}$ and other clusters near the onset of nanoparticle metallicity may provide unexpected opportunities to discover and tailor nanoscale magnetic and spin properties. In addition, these monolayer-protected clusters are likely to provide key insights into the evolution of nanoparticle electronic and magnetic properties as domain size approaches bulk-like responses.

EXPERIMENTAL METHODS

The $Au_{25}(SC_8H_9)_{18}$, $Au_{144}(SC_8H_9)_{60}$, and $Au_{459}(pMBA)_{170}$ MPCs were synthesized according to previously reported protocols.[19] $Au_{459}(pMBA)_{170}$ was prepared for MCD measurements by dispersing the nanocluster in a solution of 10% poly(vinyl alcohol) in water. $Au_{25}(SC_8H_9)_{18}$ and $Au_{144}(SC_8H_9)_{60}$ MPCs were dispersed in a solution of 10% polystyrene in toluene. Each sample solution was dropcast onto a quartz coverslip, and a second coverslip was applied to the top surface, confining a thin layer of sample solution between the coverslips. The sample was then dried completely in a vacuum desiccator and adhered to the sample cryostat probe using adhesive copper tape. The sample-loaded probe was inserted into the sample chamber of a cryogenically cooled superconducting 10-T magnet (Oxford). Low-temperature measurements were performed using 3He in the sample space to cool the MPCs to temperatures as low as 0.36 K. Variable temperatures were controlled using a resistive heater attached to the sample probe. Absorption and MCD measurements were carried out using the output of a quartz-tungsten-halogen (QTH) 250 W lamp (Newport). The lamp wavelength was scanned using a monochromator and focused to the sample. The light polarization state was modulated using a photoelastic modulator. Differential absorption of circularly polarized light at each scanned wavelength for different sample temperatures and applied field strengths was detected using a Si photodiode. A lock-in amplifier was used to synchronize absorption events to specific polarization states.

ASSOCIATED CONTENT

Supporting Information

The Supporting Information is available free of charge at https://pubs.acs.org/doi/10.1021/acs.jpclett.3c01170.

Calculated Landé g-factors, raw temperature-dependent MCD spectra, field-dependent MCD spectra, MCD magnetization curves (PDF)

AUTHOR INFORMATION

Corresponding Author

Kenneth L. Knappenberger, Jr. − *Department of Chemistry, Pennsylvania State University, University Park, Pennsylvania 16802, United States;* orcid.org/0000-0003-4123-3663; Email: klk260@psu.edu

Authors

Juniper Foxley − *Department of Chemistry, Pennsylvania State University, University Park, Pennsylvania 16802, United States*

Thomas D. Green − *Department of Chemistry, Bucknell University, Lewisburg, Pennsylvania 17837, United States*

Marcus A. Tofanelli − *Department of Chemistry, Colorado State University, Fort Collins, Colorado 80523, United States*

Christopher J. Ackerson − *Department of Chemistry, Colorado State University, Fort Collins, Colorado 80523, United States;* orcid.org/0000-0001-6863-6054

Complete contact information is available at: https://pubs.acs.org/10.1021/acs.jpclett.3c01170

Author Contributions

J.F. and T.D.G. have contributed equally.

Notes

The authors declare no competing financial interest.

ACKNOWLEDGMENTS

This work was supported by a grant from the Air Force Office of Scientific Research (FA9550-22-1-0402). J.F. acknowledges support from the National Science Foundation, award CHE-22-04190. C.J.A. acknowledges support from the National Science Foundation, award CHE-1507646.

REFERENCES

(1) Valden, M.; Lai, X.; Goodman, D. W. Onset of Catalytic Activity of Gold Clusters on Titania with the Appearance of Nonmetallic Properties. *Science* **1998**, *281* (5383), 1647−1650.

(2) Hirsch, L. R.; Stafford, R. J.; Bankson, J. A.; Sershen, S. R.; Rivera, B.; Price, R. E.; Hazle, J. D.; Halas, N. J.; West, J. L. Nanoshell-mediated near-infrared thermal therapy of tumors under magnetic resonance guidance. *Proc. Natl. Acad. Sci. U.S.A.* **2003**, *100* (23), 13549−13554.

(3) Sardar, R.; Funston, A. M.; Mulvaney, P.; Murray, R. W. Gold Nanoparticles: Past, Present, and Future. *Langmuir* **2009**, *25* (24), 13840−13851.

(4) Chen, L.-Y.; Wang, C.-W.; Yuan, Z.; Chang, H.-T. Fluorescent Gold Nanoclusters: Recent Advances in Sensing and Imaging. *Anal. Chem.* **2015**, *87* (1), 216−229.

(5) Li, G.; Jin, R. Atomically Precise Gold Nanoclusters as New Model Catalysts. *Acc. Chem. Res.* **2013**, *46* (8), 1749−1758.

(6) Zhao, T.; Herbert, P. J.; Zheng, H.; Knappenberger, K. L. State-Resolved Metal Nanoparticle Dynamics Viewed through the Combined Lenses of Ultrafast and Magneto-optical Spectroscopies. *Acc. Chem. Res.* **2018**, *51* (6), 1433−1442.

(7) Compel, W. S.; Wong, O. A.; Chen, X.; Yi, C.; Geiss, R.; Häkkinen, H.; Knappenberger, K. L.; Ackerson, C. J. Dynamic Diglyme-Mediated Self-Assembly of Gold Nanoclusters. *ACS Nano* **2015**, *9* (12), 11690−11698.
(8) Jarrett, J. W.; Zhao, T.; Johnson, J. S.; Knappenberger, K. L. J. Investigating Plasmonic Structure-Dependent Light Amplification and Electronic Dynamics Using Advances in Nonlinear Optical Microscopy. *J. Phys. Chem. C* **2015**, *119* (28), 15779−15800.
(9) Foxley, J.; Knappenberger, K. L. Magneto-Optical Properties of Noble Metal Nanostructures. *Annu. Rev. Phys. Chem.* **2023**, *74*, 53.
(10) Zaitoun, M. A.; Mason, W. R.; Lin, C. T. Magnetic Circular Dichroism Spectra for Colloidal Gold Nanoparticles in Xerogels at 5.5 K. *J. Phys. Chem. B* **2001**, *105* (29), 6780−6784.
(11) Yao, H.; Shiratsu, T. Multipolar Surface Magnetoplasmon Resonances in Triangular Silver Nanoprisms studied by MCD Spectroscopy. *J. Phys. Chem. C* **2017**, *121* (1), 761−768.
(12) Han, B.; Gao, X.; Shi, L.; Zheng, Y.; Hou, K.; Lv, J.; Guo, J.; Zhang, W.; Tang, Z. Geometry-Modulated Magnetoplasmonic Optical Activity of Au Nanorod-Based Nanostructures. *Nano Lett.* **2017**, *17* (10), 6083−6089.
(13) Negishi, Y.; Tsunoyama, H.; Suzuki, M.; Kawamura, N.; Matsushita, M. M.; Maruyama, K.; Sugawara, T.; Yokoyama, T.; Tsukuda, T. X-ray Magnetic Circular Dichroism of Size-Selected, Thiolated Gold Clusters. *J. Am. Chem. Soc.* **2006**, *128* (37), 12034−12035.
(14) Karimova, N. V.; Aikens, C. M. Optical Properties of Small Gold Clusters $Au_8L_8^{2+}$ (L = PH_3, PPh_3): Magnetic Circular Dichroism Spectra. *J. Phys. Chem. C* **2017**, *121* (35), 19478−19489.
(15) Jaw, H. R. C.; Mason, W. R. Electronic absorption and MCD spectra for the octakis(triphenylphosphine)octagold(2+) ion. *Inorg. Chem.* **1991**, *30* (18), 3552−3555.
(16) Herbert, P. J.; Window, P.; Ackerson, C. J.; Knappenberger, K. L. Low-Temperature Magnetism in Nanoscale Gold Revealed through Variable-Temperature Magnetic Circular Dichroism Spectroscopy. *J. Phys. Chem. Lett.* **2019**, *10* (2), 189−193.
(17) Herbert, P. J.; Tofanelli, M. A.; Ackerson, C. J.; Knappenberger, K. L. The Influence of Pd-Atom Substitution on $Au_{25}(SC_8H_9)_{18}$ Cluster Photoluminescence. *J. Phys. Chem. C* **2021**, *125* (13), 7267−7275.
(18) Green, T. D.; Herbert, P. J.; Yi, C.; Zeng, C.; McGill, S.; Jin, R.; Knappenberger, K. L. Characterization of Emissive States for Structurally Precise $Au_{25}(SC_8H_9)_{18}^0$ Monolayer-Protected Gold Nanoclusters Using Magnetophotoluminescence Spectroscopy. *J. Phys. Chem. C* **2016**, *120* (31), 17784−17790.
(19) Yi, C.; Zheng, H.; Howard, L. M.; Ackerson, C. J.; Knappenberger, K. L. Nanometals: Identifying the Onset of Metallic Relaxation Dynamics in Monolayer-Protected Gold Clusters Using Femtosecond Spectroscopy. *J. Phys. Chem. C* **2015**, *119* (11), 6307−6313.
(20) Akola, J.; Walter, M.; Whetten, R. L.; Häkkinen, H.; Grönbeck, H. On the Structure of Thiolate-Protected Au_{25}. *J. Am. Chem. Soc.* **2008**, *130* (12), 3756−3757.
(21) Zhu, M.; Aikens, C. M.; Hendrich, M. P.; Gupta, R.; Qian, H.; Schatz, G. C.; Jin, R. Reversible Switching of Magnetism in Thiolate-Protected Au_{25} Superatoms. *J. Am. Chem. Soc.* **2009**, *131* (7), 2490−2492.
(22) Zhu, M.; Eckenhoff, W. T.; Pintauer, T.; Jin, R. Conversion of Anionic $[Au_{25}(SCH_2CH_2Ph)_{18}]^-$ Cluster to Charge Neutral Cluster via Air Oxidation. *J. Phys. Chem. C* **2008**, *112* (37), 14221−14224.
(23) Ingram, R. S.; Hostetler, M. J.; Murray, R. W.; Schaaff, T. G.; Khoury, J. T.; Whetten, R. L.; Bigioni, T. P.; Guthrie, D. K.; First, P. N. 28 KDa Alkanethiolate-Protected Au Clusters Give Analogous Solution Electrochemistry and STM Coulomb Staircases. *J. Am. Chem. Soc.* **1997**, *119* (39), 9279−9280.
(24) Yi, C.; Tofanelli, M. A.; Ackerson, C. J.; Knappenberger, K. L. Optical Properties and Electronic Energy Relaxation of Metallic $Au_{144}(SR)_{60}$ Nanoclusters. *J. Am. Chem. Soc.* **2013**, *135* (48), 18222−18228.
(25) Jensen, K. M. Ø.; Juhas, P.; Tofanelli, M. A.; Heinecke, C. L.; Vaughan, G.; Ackerson, C. J.; Billinge, S. J. L. Polymorphism in magic-sized $Au_{144}(SR)_{60}$ Clusters. *Nat. Commun.* **2016**, *7* (1), 11859.
(26) Yan, N.; Xia, N.; Liao, L.; Zhu, M.; Jin, F.; Jin, R.; Wu, Z. Unraveling the long-pursued Au_{144} Structure by x-ray crystallography. *Sci. Adv.* **2018**, *4* (10), No. eaat7259.
(27) Weissker, H.-C.; Escobar, H. B.; Thanthirige, V. D.; Kwak, K.; Lee, D.; Ramakrishna, G.; Whetten, R. L.; López-Lozano, X. Information on quantum states pervades the visible spectrum of the ubiquitous $Au_{144}(SR)_{60}$ gold nanocluster. *Nat. Commun.* **2014**, *5* (1), 3785.
(28) Zhou, M.; Zeng, C.; Chen, Y.; Zhao, S.; Sfeir, M. Y.; Zhu, M.; Jin, R. Evolution from the plasmon to exciton state in ligand-protected atomically precise gold nanoparticles. *Nat. Commun.* **2016**, *7* (1), 13240.
(29) Kwak, K.; Thanthirige, V. D.; Pyo, K.; Lee, D.; Ramakrishna, G. Energy Gap Law for Exciton Dynamics in Gold Cluster Molecules. *J. Phys. Chem. Lett.* **2017**, *8* (19), 4898−4905.
(30) Negishi, Y.; Nakazaki, T.; Malola, S.; Takano, S.; Niihori, Y.; Kurashige, W.; Yamazoe, S.; Tsukuda, T.; Häkkinen, H. A Critical Size for Emergence of Nonbulk Electronic and Geometric Structures in Dodecanethiolate-Protected Au Clusters. *J. Am. Chem. Soc.* **2015**, *137* (3), 1206−1212.
(31) Mason, W. R. *A Practical Guide to Magnetic Circular Dichroism Spectroscopy*; John Wiley & Sons, Ltd: Hoboken, 2006.
(32) Neese, F.; Solomon, E. I. MCD C-Term Signs, Saturation Behavior, and Determination of Band Polarizations in Randomly Oriented Systems with Spin $S \geq 1/2$. Applications to $S = 1/2$ and $S = 5/2$. *Inorg. Chem.* **1999**, *38* (8), 1847−1865.
(33) Zhu, M.; Aikens, C. M.; Hollander, F. J.; Schatz, G. C.; Jin, R. Correlating the Crystal Structure of a Thiol-Protected Au_{25} Cluster and Optical Properties. *J. Am. Chem. Soc.* **2008**, *130* (18), 5883−5885.
(34) Malola, S.; Lehtovaara, L.; Häkkinen, H. TDDFT Analysis of Optical Properties of Thiol Monolayer-Protected Gold and Intermetallic Silver−Gold $Au_{144}(SR)_{60}$ and $Au_{84}Ag_{60}(SR)_{60}$ Clusters. *J. Phys. Chem. C* **2014**, *118* (34), 20002−20008.
(35) Zheng, H.; Tofanelli, M. A.; Ackerson, C. J.; Knappenberger, K. L. Composition-dependent electronic energy relaxation dynamics of metal domains as revealed by bimetallic $Au_{144-x}Ag_x(SC_8H_9)_{60}$ mo nolayer-protected clusters. *Phys. Chem. Chem. Phys.* **2017**, *19* (22), 14471−14477.
(36) Schatz, P. N.; Mowery, R. L.; Krausz, E. R. M.C.D./M.C.P.L. saturation theory with application to molecules in $D_{\infty h}$ and its subgroups. *Mol. Phys.* **1978**, *35* (6), 1537−1557.
(37) Mack, J.; Stillman, M. J. Magnetic Circular Dichroism (MCD) Spectroscopy. In *Encyclopedia of Inorganic Chemistry*; King, R. B., Crabtree, R. H., Lukehart, C. M., Atwood, D. A., Scott, R. A., Eds.; John Wiley & Sons, Ltd, 2008; pp 189−204.
(38) Reber, A. C.; Khanna, S. N. Superatoms: Electronic and Geometric Effects on Reactivity. *Acc. Chem. Res.* **2017**, *50* (2), 255−263.
(39) *Superatoms: Principles, Synthesis and Applications*; Jena, P., Sun, Q., Eds.; John Wiley & Sons, Ltd, 2021.
(40) Häkkinen, H. Atomic and electronic structure of gold clusters: understanding flakes, cages and superatoms from simple concepts. *Chem. Soc. Rev.* **2008**, *37* (9), 1847−1859.
(41) Jiang, D. E.; Kühn, M.; Tang, Q.; Weigend, F. Superatomic Orbitals under Spin-Orbit Coupling. *J. Phys. Chem. Lett.* **2014**, *5* (19), 3286−3289.
(42) Green, T. D.; Yi, C.; Zeng, C.; Jin, R.; McGill, S.; Knappenberger, K. L. Temperature-Dependent Photoluminescence of Structurally-Precise Quantum-Confined $Au_{25}(SC_8H_9)_{18}$ and $Au_{38}(SC_{12}H_{25})_{24}$ Metal Nanoparticles. *J. Phys. Chem. A* **2014**, *118* (45), 10611−10621.
(43) Malola, S.; Kaappa, S.; Häkkinen, H. Role of Nanocrystal Symmetry in the Crossover Region from Molecular to Metallic Gold Nanoparticles. *J. Phys. Chem. C* **2019**, *123* (33), 20655−20663.

https://doi.org/10.1021/acs.jpclett.3c01170
J. Phys. Chem. Lett. 2023, 14, 5210−5215